Structure and hydrogen content of polymorphous silicon thin films studied by spectroscopic ellipsometry and nuclear measurements

A. Fontcuberta i Morral and P. Roca i Cabarrocas*
Laboratoire de Physique des Interfaces et des Couches Minces (UMR 7647 CNRS), Ecole Polytechnique, F-91128 Palaiseau Cedex, France

C. Clerc
CSNSM, Bâtiment 108, Université Paris Sud, 91405 Orsay Campus, France
(Received 24 July 2003; published 10 March 2004)

The dielectric functions of amorphous and polymorphous silicon films prepared under various plasma conditions have been deduced from UV-visible spectroscopic ellipsometry measurements. The measured spectra have been first simulated by the use of the Tauc-Lorentz dispersion model and then the compositions of the films have been obtained by the use of the tetrahedron model combined with the Bruggeman effective medium approximation. This approach allows us to determine the hydrogen content, the crystalline fraction, and the void fraction of the films. This is particularly important in the case of polymorphous films in which the low crystalline fraction (below 10%) can only be detected when an accurate description of the effects of hydrogen on the dielectric function through the tetrahedron model is considered. The hydrogen content and film porosity deduced from the analysis of the spectroscopic ellipsometry measurements are in excellent agreement with the hydrogen content and film density deduced from combined elastic recoil detection analysis and Rutherford backscattering spectroscopy measurements. Moreover, despite their high hydrogen content (~15%–20%) with respect to hydrogenated amorphous silicon films deposited at the same temperature (8%), polymorphous silicon films have a high density, which is related to their very low void fraction.

DOI: 10.1103/PhysRevB.69.125307 PACS number(s): 68.55.Nq, 78.20.Bh, 78.40.Fy, 81.15.Gh

I. INTRODUCTION

Plasma deposition of silicon thin films is an expanding field driven by an increasing number of applications. They relay on the possibility of producing materials covering a wide range of optical and electrical properties ranging from disordered materials such as amorphous silicon (a-Si:H) to more ordered films such as microcrystalline silicon (μc-Si:H). Recently, there has been a strong interest in producing materials at the border line between a-Si:H and μc-Si:H. In particular polymorphous silicon (pm-Si:H),[1,2] protocrystalline silicon,[3] and paracrystalline silicon.[4] Based on *in situ* ellipsometry studies we have shown that polymorphous and protocrystalline silicon are different materials, the difference resulting from the growth process.[5] Protocrystalline silicon corresponds to an intermediate state in the dynamic process of the formation of microcrystalline silicon, i.e., for fixed plasma conditions, protocrystalline films can be achieved only in a certain thickness range.[6] On the contrary homogenous pm-Si:H films can be achieved at any thickness (up to 10 microns).[7] As these materials are intermediate between amorphous and microcrystalline, the main difficulty is to find an adequate way of characterizing their particular structure. From optical transmission measurements it has been shown that pm-Si:H films have a higher refractive index and wider optical gap than a-Si:H,[8] while with Raman spectroscopy it has been possible to detect the presence of a small volume fraction of nanometer size crystallites,[9] which have also been detected in high resolution transmission electron microscopy studies.[10] These subtle changes in the structure of pm-Si:H films contrast with the larger ones observed in their electronic properties such as a very low defect density and higher diffusion length of minority carriers compared to a-Si:H.[11,12] Thus, a detailed characterization of the film structure is necessary to better understand the origin of the improved transport properties.

UV-visible spectroscopic ellipsometry (SE) is a powerful technique commonly used to characterize a-Si:H and μc-Si:H materials.[13,14] However, its application to films containing small amounts of nanometer sized silicon particles in a silicon matrix has failed so far. Moreover, the use of effective medium models to describe the dielectric function of mixed phase materials faces the problem of having an independent measure of the dielectric function of the inclusions. Few attempts have been made to determine the dielectric function of small crystallites and the reported values are probably largely dependent on the film deposition method.[15] Besides the small amount of crystallites, pm-Si:H films have a higher hydrogen content and some specific hydrogen bands detected by infrared and hydrogen evolution measurements.[16] However, in the modeling of the dielectric function, the effect of hydrogen is generally omitted. Nevertheless hydrogen has many effects in silicon films such as (i) the reconstruction of weak Si–Si bonds, (ii) the local densification of the amorphous network due to shorter length of the Si–H bond in comparison to the Si–Si bond, (iii) the lowering of network cross-linking due to an enhancement of void formation, and (iv) an increase of the density of states in the conduction band due to the antibonding states of the Si–H bond. All these effects will influence the film dielectric function as observed experimentally[17] and thus the effect of hydrogen should be considered in a detailed modeling of the film dielectric function.

In this paper we present a comprehensive study of the dielectric function of amorphous and polymorphous silicon thin films using the tetrahedron model[18] and the Bruggeman effective medium approximation (BEMA).[19] This approach has been already applied to amorphous silicon films[20] and allows the quantification of hydrogen, void, and crystalline fractions of the films, which we compare to the hydrogen content and film density deduced from elastic recoil detection analysis (ERDA) and Rutherford backscattering spectroscopy (RBS) measurements.

The structure of the paper is as follows: the experiments are described in Sec. II. In Sec. III we present a detailed description of the tetrahedron model and the methodology used in the analysis of the dielectric function. The proposed methodology is validated for amorphous silicon films (Sec. IV A), where the results of the model are checked against those deduced from RBS and ERDA measurements, and then extended to pm-Si:H and protocrystalline films with low crystalline fractions (Sec. IV B). In Sec. V we discuss the benefits of the proposed methodology to model the dielectric function of silicon thin films at the edge of crystallization as well as the particular features of polymorphous films. Finally, Sec. VI summarizes the results.

II. EXPERIMENTS

Silicon thin films were deposited by plasma enhanced chemical vapor deposition. Standard hydrogenated amorphous silicon (a-Si:H) was obtained by the decomposition of pure silane at low pressure and low rf power (6 Pa and 17 mW/cm^2). In order to vary the hydrogen and void contents, a series of films was deposited at different substrate temperatures ranging from 50 °C to 300 °C. Protocrystalline and polymorphous silicon were produced by the dissociation of 6% silane in hydrogen gas mixtures under an rf power of 100 mW/cm^2. The total gas pressure was varied between 53 and 240 Pa. Both electrodes were maintained at 250 °C. At this dilution and temperature, the transition from μc-Si:H to pm-Si:H takes place at ~80 Pa. All the films were measured after deposition by spectroscopic ellipsometry at room temperature. The dielectric function of the films was analyzed using the Tauc-Lorentz model. From this parametric modeling we obtained the dielectric function of the films, their thickness and roughness. To obtain quantitative information on the hydrogen content and the crystalline fraction we combined the BEMA with the tetrahedron model as shown in the next section.

Rutherford backscattering spectroscopy (RBS) and elastic recoil detection analysis (ERDA) measurements were performed to obtain the density and hydrogen content of the films. For an accurate determination of the density, the films were deposited on a 400 Å thin chromium layer thermally evaporated on a crystalline silicon substrate. This allows us to separate in the RBS spectra the response of silicon atoms of the film from those of the silicon substrate. A monokinetic beam of He^+ ions at 1.5 MeV was used for RBS. The peak integration provides the number of Si atoms per cm^2 by comparison to a standard sample. Knowing the thickness of the silicon film from ellipsometry measurements, the density was deduced. In the case of ERDA, the sample was bombarded with a monokinetic beam of He^{2+} ions at 3 MeV. The number of ejected hydrogen atoms is proportional to the concentration of hydrogen in the sample. The proportionality factor was calculated before each experiment by measuring the number of recoils from a reference sample, whose hydrogen concentration is known.

TABLE I. Scaling parameters used by Mui *et al.* in the calculation of the dielectric function of the three types of hydrogenated tetrahedra.

Tetrahedra	C_{1n}	C_{2n}
$Si–Si_4$	1	1
$Si–Si_3H$	0.864	0.786
$Si–Si_2H_2$	0.681	0.6
$Si–SiH_3$	0.493	0.445

III. THE TETRAHEDRON MODEL

The tetrahedron model was first derived by Mui *et al.* to understand the role of hydrogen in the optical properties of hydrogenated amorphous silicon.[21,22] The network of a-Si:H is assumed to consist of an ensemble of voids and silicon centered tetrahedra, whose vertices can be either silicon or hydrogen atoms, and symbolized by: $Si–Si_{4-n}H_n$ ($n=0,1,2,3$), SiH_4 being excluded from the model. The dielectric function of the n-hydrogenated tetrahedra, ε_n, is derived by the scaling relation,

$$\tilde{\varepsilon}_n - 1 = C_{1n}(\mathcal{E}_{a\text{-Si}}(C_{2n}.E) - 1). \quad (1)$$

$\mathcal{E}_{a\text{-Si}}$ is the dielectric function of hydrogen free and dense amorphous silicon, which is taken as the dielectric function of $Si–Si_4$. C_{1n} and C_{2n} are scaling parameters, whose values are given in Table I, taken from Ref. 18.

Figure 1 shows the real and imaginary parts of the dielectric functions of a-Si, $Si–Si_3H$, and $Si–Si_2H_2$ derived from this scaling relation. Replacing Si–Si bonds by stronger Si–H bonds shifts the spectra to higher energies and slightly lowers the values of the maxima of the real and imaginary part of $\tilde{\varepsilon}$. The volume fraction of each tetrahedra is calculated as a function of the composition x of the $Si_{1-x}H_x$ film. First, the probability P_n of presence of each type of tetrahedron is calculated as a function of x, assuming a random distribution of bonded hydrogen. Then, the volume V_n of each n tetrahedron is derived from simple geometric relations on the basis of the bond lengths: $r(\text{Si–Si}) = 1.176$ Å and $r(\text{Si–H}) = 0.74$ Å. The volume fraction f_n of an n-tetrahedron is given by

$$f_n^{(x)} = \frac{P_n^{(x)} \cdot V_n}{\Sigma_n P_n \cdot V_n}. \quad (2)$$

In Fig. 2.a the probability of presence $P_n(x)$ of each $Si–Si_{4-n}H_n$ tetrahedra as a function of the hydrogen content x of the film is shown. For hydrogen contents lower than 25% the concentration of $Si–Si_3H$ is much higher than that

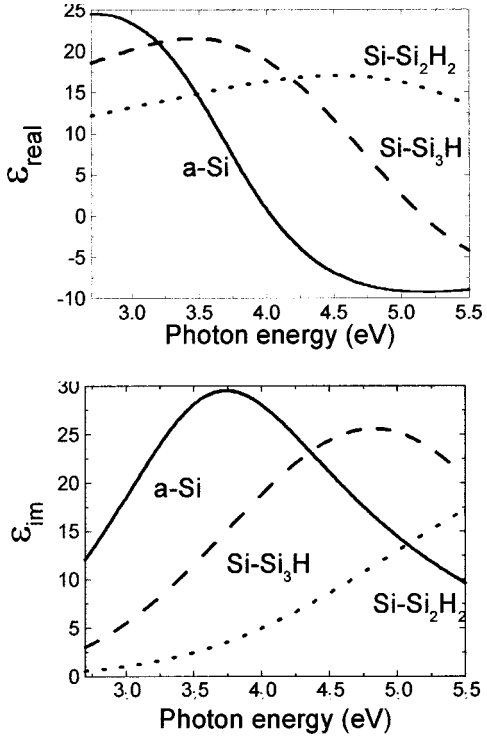

FIG. 1. Real and imaginary parts of the dielectric function of the tetrahedra containing 0, 1, and 2 hydrogen atoms.

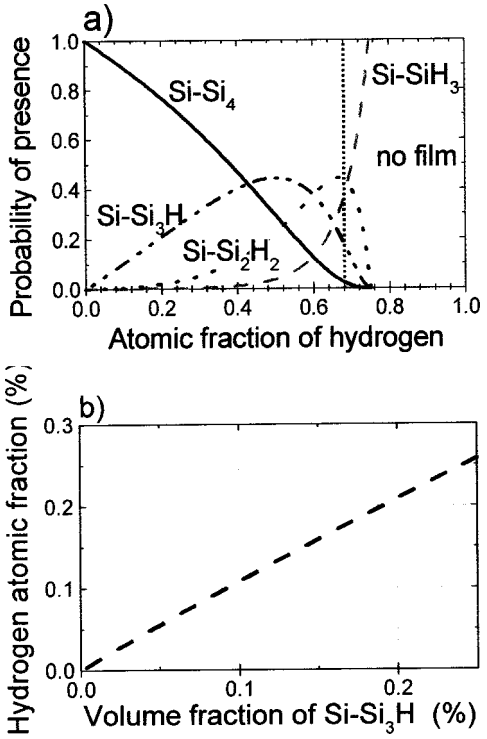

FIG. 2. Probability of presence of each $Si-Si_{4-n}H_n$ tetrahedra as a function of the atomic hydrogen content (a), and atomic hydrogen content of the film as a function of the volume fraction of $Si-Si_3H$ (b).

of $Si-Si_2H_2$ and $Si-SiH_3$, and only $Si-Si_3H$ has an effect on the optical properties. At higher hydrogen contents, the proportions of $Si-Si_2H_2$ and $Si-SiH_3$ become larger and have to be taken into account when simulating the optical properties of the film. Above 65% of hydrogen, the network is not continuous anymore and a solid film cannot exist. In our samples with hydrogen contents up to 25%, we will consider that most of the hydrogen is bonded in $Si-Si_3H$ tetrahedral units. Thus, combining the tetrahedron model with the BEMA, the effect of the incorporation of hydrogen into the silicon network can be calculated by considering *a*-Si:H as a mixture of *a*-Si, $Si-Si_3H$ and voids. In this way, we can obtain the volume fraction of $Si-Si_3H$ units, which is related to the atomic hydrogen content by Eq. (2). Such relation is plotted in Fig. 2(b).

While the observation of a high void fraction has often been associated with a high hydrogen content,[23,24] the tetrahedron model offers the possibility to distinguish between the effects of hydrogen and voids on the dielectric function and thus to quantify their respective fractions. As an example, Fig. 3 shows the effect of the void fraction on the real and imaginary parts of the dielectric function of amorphous silicon. The dielectric function given by Aspnes[25] has been taken as a reference. We can see that the increase of the void volume fraction leads to a decrease of the amplitude of the imaginary part of the dielectric function without any shift. On the contrary, the increase of the bonded hydrogen content should lead to an opening of the gap. This is clearly seen in Fig. 4 where we plot the effect of the hydrogen content on the real and imaginary parts of the dielectric function. Indeed Fig. 4 shows that the increase of hydrogen leads to a slight decrease of $\varepsilon_{\mathrm{im}}$ but also to a shift of the maximum of both $\varepsilon_{\mathrm{real}}$ and $\varepsilon_{\mathrm{im}}$ to higher photon energies. Because of their different effect on the dielectric function, both voids and bonded-hydrogen contents can be determined independently.

Methodology for the analysis the dielectric function: In this section we give a detailed example of the methodology we have developed. Spectroscopic ellipsometry measurements of thin films provide information from different depths of the sample structure. For example, at low photon energies, the penetration depth can be larger than the film thickness, which leads to interference fringes as shown in Fig. 5(a). With increasing photon energy, the penetration depth decreases until the film is opaque and the influence of the surface roughness becomes dominant. The optical response of the multilayer structure is calculated by the generalization of the Fresnel laws.[26] The SE data are analyzed taking into account the substrate, the thin film, and its surface roughness. Each layer has its own dielectric function, and that of the substrate is known or determined by SE measurements performed before deposition. The surface roughness is considered as an overlayer formed by a mixture of 50% bulk material and 50% voids. To describe the dielectric function of the bulk two approaches can be used:

(i) To use dispersion laws. In the case of amorphous silicon, the Tauc-Lorentz model allows to achieve excellent fit of the dielectric function.

(ii) Bruggemann effective medium approximation in which the measured pseudodielectric function is described by the sum of the dielectric function of the

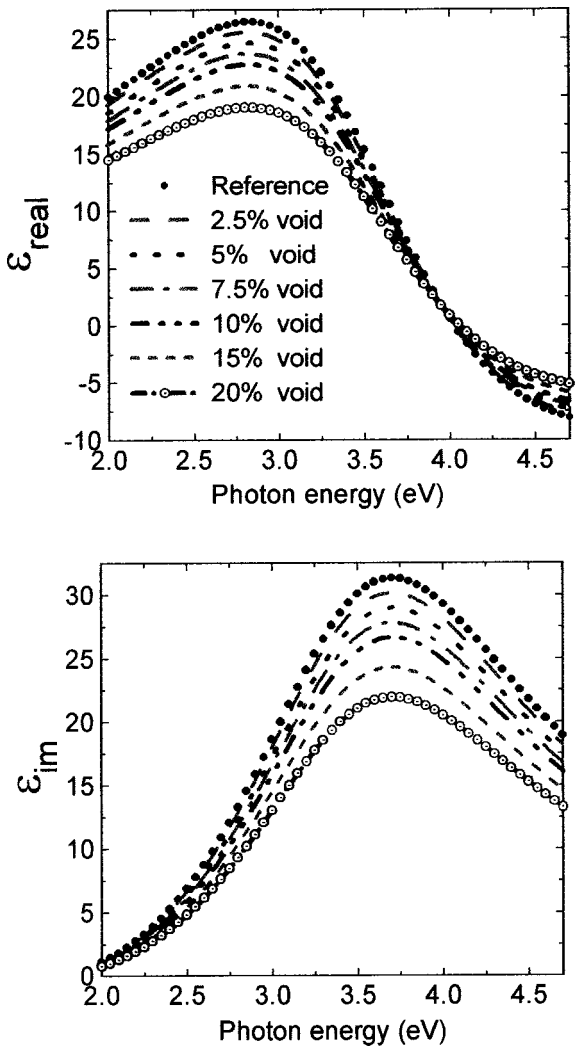

FIG. 3. Effect of the void fraction on the dielectric function of amorphous silicon simulated with BEMA. The dielectric function used as the reference for *a*-Si is the one reported by Aspness (Ref. 25).

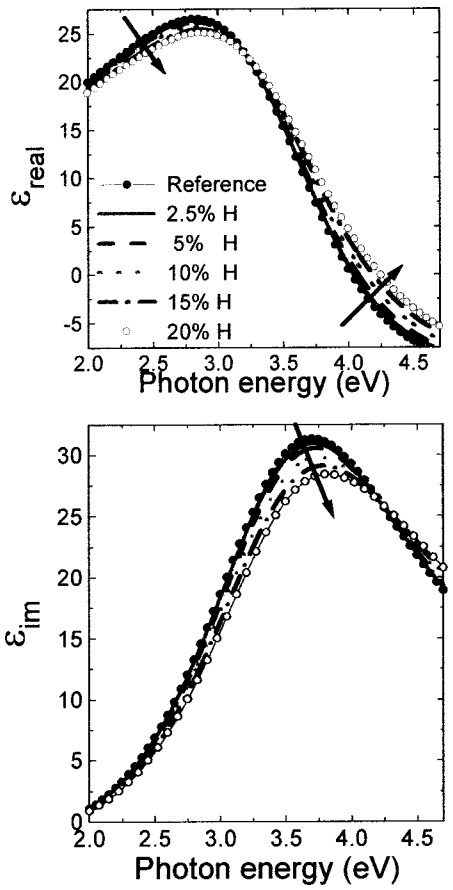

FIG. 4. Effect of the hydrogen content on the dielectric function of hydrogenated amorphous silicon simulated combining the BEMA and the tetrahedron model. The arrows indicate the shift of the dielectric function.

film constituents averaged by their respective volume fractions. The dielectric function of each constituent is taken from a library.[27]

While BEMA is well adapted in cases where the dielectric function of the constituents is precisely known, it is less accurate for materials like hydrogenated amorphous and polymorphous silicon whose dielectric function is strongly dependent on their hydrogen content. In Fig. 5 we compare the two approaches: the standard BEMA where the dielectric function of the bulk layer is considered as a mixture of 95% amorphous silicon[28] and 5% voids, and the Tauc-Lorentz where we calculate the exact dielectric function of the film. As shown in Fig. 5(a) the standard BEMA approach does not reproduce the experimental data, particularly in the low energy part of the spectrum. On the contrary, the use of a dispersion law for the dielectric function allows a perfect fit to the experimental data. In this case, the dielectric function is described by the Tauc-Lorentz dispersion law.[29] Considering only a single transition, the imaginary part of the dielectric function is obtained multiplying the equation of the Lorentz oscillator by the equation of the Tauc joint density of states, which gives:

$$\varepsilon_{\mathrm{im\,TL}}(E)=\frac{A\cdot E_0\cdot C\cdot(E-E_g)^2}{(E^2-E_g)^2+C^2\cdot E^2}\cdot\frac{1}{E}\quad E>E_g\,, \tag{3}$$

$$\varepsilon_{\mathrm{im\,TL}}(E)=0\quad E\leqslant E_g\,, \tag{4}$$

where E_0 is the peak transition energy, E_g is the gap energy, and C a broadening parameter, which can be related to the degree of disorder in the material. A is another parameter which is proportional to the height of $\varepsilon_{\mathrm{im}}$, related to the film density. There is an additional parameter, it is the value of the real part of $\tilde{\varepsilon}$ at infinite energy, $\varepsilon_{\mathrm{real}\,\infty}$, which is related to $\varepsilon_{\mathrm{im}}$ through the Kramers-Kronig relation. In the example of Fig. 5(a) the values of the parameters are $E_g=1.70$ eV, $\varepsilon_{\mathrm{real}\,\infty}=0.22$, $E_0=3.62$ eV, $A=229$, and $C=2.13$ eV.

In Fig. 5(b) we compare the dielectric function of the film deduced from both approaches. The differences between both $\tilde{\varepsilon}$ are evident, particularly in the region of the absorption edge and the maximum. We can see that the BEMA model without hydrogen gives a redshifted absorption edge, which is not the case with the use of the Tauc-Lorentz dis-

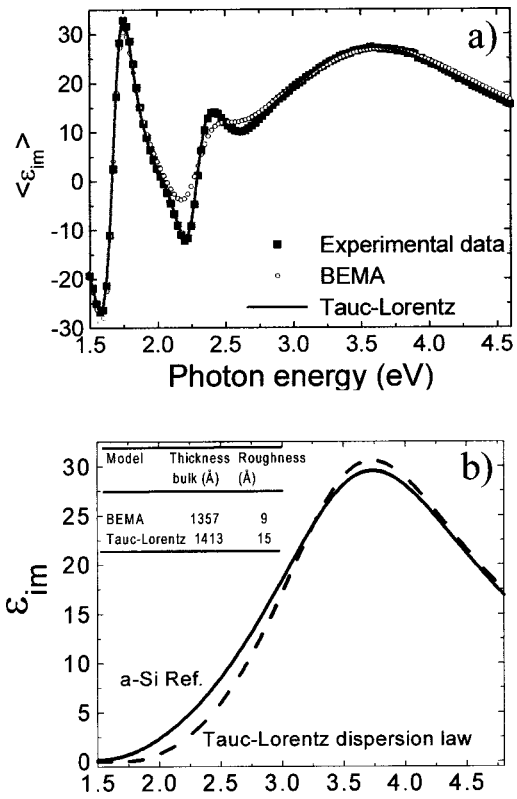

FIG. 5. Imaginary part of the pseudodielectric function of a polymorphous silicon thin film on glass measured by spectroscopic ellipsometry (black squares) and the results of two models: The open circles represent the model obtained with the standard BEMA using a reference for *a*-Si and voids; and the gray line the results obtained using the Tauc-Lorentz dispersion law (a). From the analysis, the thickness of the film and its roughness can be deduced. The results of the two kinds of analysis are shown in the inset of (b), where we compare the imaginary part of the dielectric function of the film obtained with the Tauc-Lorentz dispersion law and the reference dielectric function of *a*-Si.

persion law. This discrepancy can be related to the fact that in the BEMA model, with only *a*-Si and voids, we cannot obtain a blueshift of the dielectric function (see Fig. 3), while one should expect a shift to high energy (Fig. 4) if the film has hydrogen. The thickness of the film deduced from both approaches is shown in the inset of Fig. 5(b). It is remarkable that in the standard approach, even using an inexact $\tilde{\varepsilon}$ of the bulk layer, the thickness has only a 7% discrepancy. This slight effect contrasts with the differences in the calculated dielectric function.

Therefore, for a more accurate analysis of the spectroscopic ellipsometry data we propose the following methodology: first, to obtain the dielectric function of the film by the Tauc-Lorentz model, which then will be used to compare to the dielectric function of materials prepared under different conditions. In this way the effects of the substrate and surface roughness can be eliminated and thus the true dielectric function of the material obtained. Second, to combine the Bruggeman effective medium approximation and the tetrahedron model to take into account the effect of hydrogen on the dielectric function, and thus achieve a more accurate description in terms of the film constituents. In our study, we will use the dielectric function of our standard *a*-Si:H deposited at 250 °C as a reference. This choice is motivated by the fact that this film has the highest density and lowest hydrogen content.

In summary, our method consists of three main steps:

(1) Derivation of the dielectric function of the film using the Tauc-Lorentz relation.
(2) Simulation of the obtained bulk $\tilde{\varepsilon}$ as a mixture of our *a*-Si:H reference, Si–Si_3H and voids in order to calculate the relative increase in hydrogen and void fraction. Moreover a volume crystalline fraction can be added to model the dielectric function of films deposited close to microcrystalline conditions. As shown below, the improved description of the dielectric function achieved by the introduction of hydrogen allows the detection of small crystalline fractions.
(3) Calculation of the absolute hydrogen and void concentration of the sample.

As an example, the dielectric function of the film shown in Fig. 5 was modeled as a mixture of 92.5% of the reference *a*-Si:H, 7% of Si–Si_3H, and 0.5% of voids. This gives an absolute hydrogen concentration of 14.4%, in very good agreement with the 15% obtained by elastic recoil detection analysis measurements.

IV. RESULTS

In the next sections amorphous, polymorphous, and protocrystalline silicon thin films are studied using the method explained above. The structure of each section is the following: first, we present the experimental spectroscopic ellipsometry data. Second, we apply the Tauc-Lorentz model to deduce the thickness, the surface roughness and the parameters of the model, which allow to obtain the true dielectric function of the material. Third, we apply the BEMA model to the calculated dielectric functions to determine the hydrogen content, the void fraction and the crystalline fraction of the films. Finally, the hydrogen contents deduced from SE are compared to these deduced from ERDA and the void fractions to the film densities deduced from RBS measurements.

A. Application to hydrogenated amorphous silicon films

Figure 6 shows the effect of the substrate temperature on the imaginary part of the pseudodielectric function of hydrogenated amorphous silicon films. We can see that decreasing the temperature results in a marked decrease of the amplitude of $\langle \varepsilon_{\mathrm{im}} \rangle$, in particular around 3.55 eV, along with a shift of the absorption edge (energy region between 2.5 and 3.5 eV) to high energy, even though this effect is partly masked by the overall decrease on the amplitude. The observed decrease in the values of $\langle \varepsilon_{\mathrm{im}} \rangle$ with decreasing substrate temperature can be due to (i) an increase of the roughness, (ii) a decrease of the density of the film, and (iii) to an increase in the hydrogen content. The parameters of the dielectric function [see Eq. (2)] the thickness of the films and their roughness are obtained by the analysis of the spectra using the Tauc-

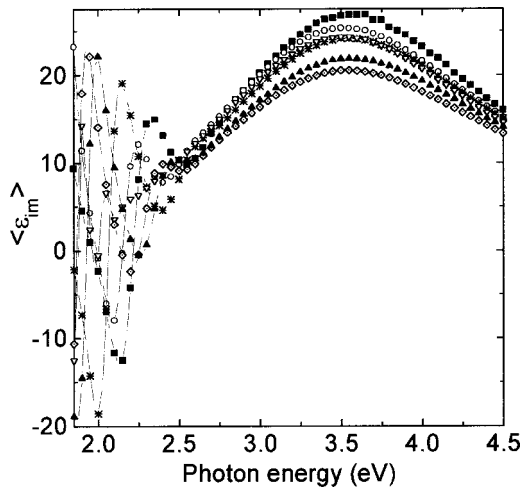

FIG. 6. Effect of the substrate temperature on the imaginary part of the pseudodielectric function of hydrogenated amorphous silicon thin films deposited under standard conditions.

Lorentz model. The values of the various parameters are reported in Table II and the dielectric function of the films is shown in Fig. 7.

As expected, the disorder in the films, characterized by the parameter C, decreases with increasing substrate temperature. The highest amplitude of the dielectric function (A) corresponds to the a-Si:H deposited at 250 °C. In this case, $\tilde{\varepsilon}$ is also the most shifted to the low energies, corresponding to the lowest values of E_0. As we will see by means of the tetrahedron model, this is related to the higher density and lower hydrogen content of the material. For the other a-Si:H films shown in Fig. 7, we observe a decrease of the amplitude and a shift of $\varepsilon_{\mathrm{im}}$ to higher energies with decreasing substrate temperature. As we will see in the following, this is related to a higher hydrogen content and void fraction with decreasing deposition temperature. However, the imaginary part of the dielectric function of the film deposited at 300 °C has a slightly lower amplitude than the one deposited at 250 °C. This is explained by the fact that hydrogen desorbs during deposition at temperatures higher than 250 °C, which leads to a more disordered and less dense film.[30]

To obtain a physical description of film microstructure, the dielectric function was modeled combining the BEMA and the tetrahedron model. The hydrogen content and void fraction deduced from this approach are shown in Table III where they are also compared to the results of ERDA and RBS measurements. We obtain a good correlation between the hydrogen contents deduced from ellipsometry and those measured by ERDA. Also the increase of the void fraction corresponds to a decrease in the film density measured by RBS. In summary, by the analysis of a series of a-Si:H films deposited at various temperatures we have validated our method to quantify the hydrogen content and void fraction of amorphous silicon. In the following section we apply it to a new material, polymorphous silicon.

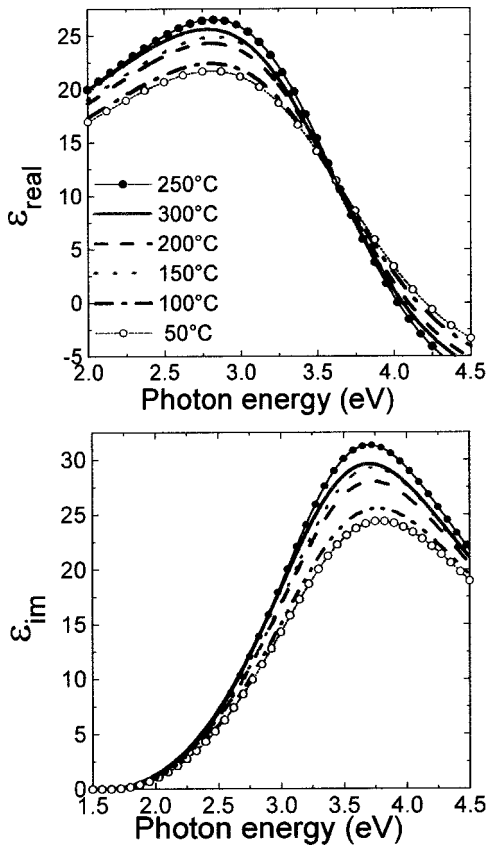

FIG. 7. Effect of the substrate temperature on the dielectric function of the a-Si:H thin films, deduced from the Tauc-Lorentz analysis of the experimental data presented in Fig. 6.

TABLE II. Effect of deposition temperature on the Tauc-Lorentz parameters of the dielectric function of a-Si:H thin films obtained by the decomposition of 6.7 Pa of pure silane.

Sample Ref.	T_s (°C)	Thickness (Å)	E_g (eV)	$\varepsilon_{1\infty}$	A	E_0 (eV)	C
904141	50	2110±15	1.65	0.46	194	3.68	2.44
904151	100	1985±15	1.65	0.24	201	3.66	2.39
904143	150	1540±15	1.62	0.34	205	3.65	2.19
904144	200	1708±15	1.66	0.17	216	3.62	2.29
010091	300	2147±15	1.62	0.29	219	3.61	2.27
904132	250	1453±15	1.65	0.01	228	3.60	2.16

TABLE III. The hydrogen content and void fractions of the a-Si:H films deduced from the analysis of the ellipsometry spectra by combining the Bruggeman effective medium approximation and tetrahedron model, compared to these deduced from ERDA and RBS, respectively.

Substrate temp (°C)	Deduced %H	Deduced % void	ERDA %H	RBS Dens. (g/cm^3)
50	18.5	11	17	2.11±0.03
100	16	9	16	2.16±0.03
150	12	3	13	2.30±0.03
200	12.5	5	12	2.29±0.03
250	Reference	0	8	2.32±0.03
300	9.5	2	9	2.26±0.03

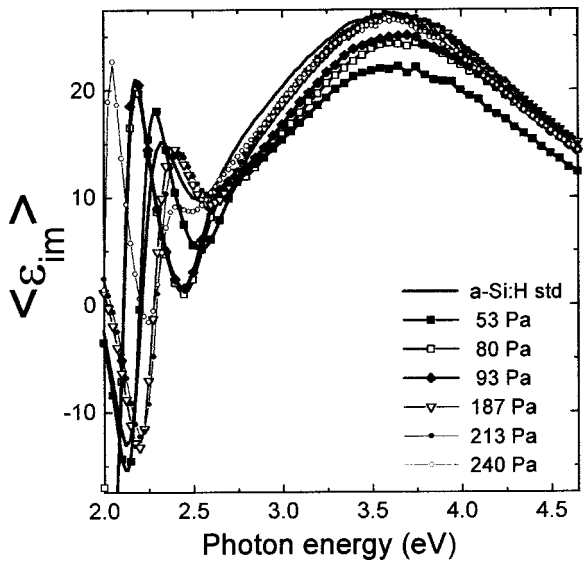

FIG. 8. Effect of gas pressure on the imaginary part of the pseudodielectric function, $\langle\varepsilon_{\mathrm{im}}\rangle$, of polymorphous silicon films deposited at 250 °C. For comparison, the $\langle\varepsilon_{\mathrm{im}}\rangle$ of a-Si:H deposited at the same temperature is also plotted.

B. Application to polymorphous silicon

Polymorphous silicon is a nanostructured material consisting of 3–4 nm size crystallites embedded in an amorphous matrix. The crystallites have been observed by high resolution transmission microscopy in a concentration ~3%.[31] It has been previously shown that their nucleation does not take place in the film itself but in the plasma phase.[32,33] Because of the low crystalline fraction we could not detect it by spectroscopic ellipsometry before the development of the tetrahedron model and has been hardly detected via Raman measurements.[9]

Figure 8 shows the imaginary part of the pseudodielectric function, $\langle\varepsilon_{\mathrm{im}}\rangle$, of the films deposited under high silane dilution conditions at various total pressures. For comparison, $\langle\varepsilon_{\mathrm{im}}\rangle$ of a-Si:H deposited at 250 °C is also plotted. At pressures ranging from 53 to 93 Pa, the material is protocrystalline, which means that thicker films deposited under the same conditions would be μc-Si:H. Indeed, a crystalline fraction of the order of 17% and 23% is obtained for these films. Such low values of the crystalline fraction cannot be detected by the standard analysis of the SE measurements. Here we show, for the first time, that smaller fractions can be detected if the dielectric function is modeled more precisely by the introduction of the tetrahedron model.

At pressures higher than 93 Pa, there is a change in the plasma regime, which modifies the nature of the species contributing to the growth and results in the obtaining of polymorphous silicon films.[33] Nevertheless, the shape and the amplitude of $\langle\varepsilon_{\mathrm{im}}\rangle$ shown in Fig. 8 are very similar to these of a-Si:H, but the maximum is shifted by 0.15 eV to higher energies. We might also note that the amplitudes of the interference fringes corresponding to pm-Si:H films are higher than those corresponding to a-Si:H. This is due to a lower absorption at low energies in the case of pm-Si:H.

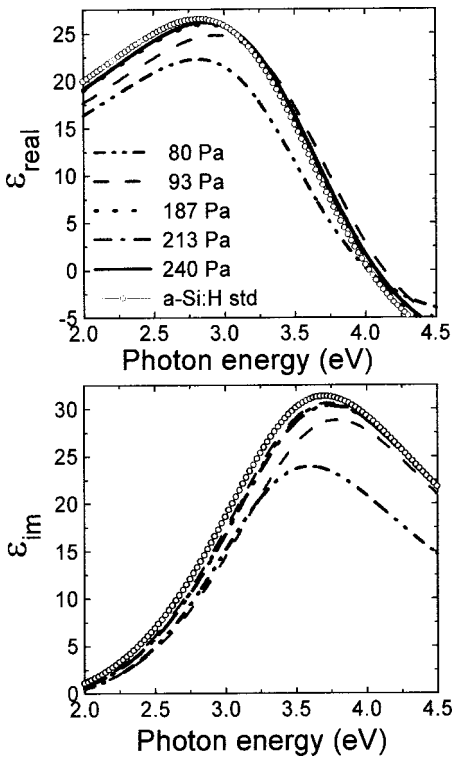

FIG. 9. Effect of the pressure on the dielectric function of silicon films obtained from the analysis of the spectra shown in Fig. 8.

The same procedure for the analysis of the dielectric function of a-Si:H in the previous section was applied to the modeling of the spectra of Fig. 8. The real and imaginary parts of the dielectric function are shown in Fig. 9. The dielectric function of an a-Si:H film deposited at 250 °C is also plotted as a reference. The $\tilde{\varepsilon}$ of the films deposited at higher pressures (pm-Si:H) look essentially the same as the $\tilde{\varepsilon}$ of a-Si:H, but shifted to higher energies. At low pressure (80 and 93 Pa) the films are protocrystalline and the amplitude of $\tilde{\varepsilon}$ is significantly lower. The values of the Tauc-Lorentz parameters corresponding to the $\tilde{\varepsilon}$ plotted in Fig. 9 are shown in Table IV. It is interesting to note that the values of E_g and E_0 of pm-Si:H films can be, respectively, up to 0.05 eV and 0.04 eV higher than the reference a-Si:H films (010091 and 010092) deposited at the same temperature. Moreover, the broadening parameter C, related to the disorder in the film, is of the same magnitude or slightly lower for pm-Si:H compared to the optimized a-Si:H.

The dielectric functions were modeled combining the BEMA and the tetrahedron model, as explained in Sec. III. The results concerning the hydrogen content and void fraction deduced by this model are shown in Table V, where they are compared to the results of ERDA and RBS measurements. As in the case of a-Si:H films (see Table III), we obtain a good correlation of the hydrogen content deduced by ellipsometry with those deduced from ERDA measurements. Moreover in some cases, like the sample deposited at 187 Pa, a low crystalline fraction of 8% had to be added for the correct simulation of the dielectric function. (see Table V). We would like to emphasize that, to our knowledge, this

TABLE IV. Effect of pressure on the Tauc-Lorentz parameters of the dielectric function of silicon thin films obtained by the decomposition a mixture of 3% of silane in hydrogen at 250 °C. The values for *a*-Si:H deposited from the decomposition of 6.7 Pa of pure silane are also given for comparison.

Sample Ref.	Pressure (Pa)	Thickness (Å)	E_g (eV)	$\varepsilon_{1\,\mathrm{inf}}$	A	E_0 (eV)	C
010043	240	2539±15	1.72	0.23	233	3.63	2.15
010042	213	1666±15	1.70	0.22	229	3.62	2.13
010036	187	1445±15	1.71	0.24	229	3.64	2.14
010032	93	1912±15	1.74	0.70	214	3.69	2.08
010031	80	1876±15	1.76	0.78	209	3.69	2.11
010024	80	2293±15	1.75	0.88	218	3.67	2.10
010023	67	1876±15	1.75	0.28	205	3.78	2.13
010022	53	1899±15	1.76	0.39	207	3.78	2.12
010091	6.7	1466±15	1.65	0.01	228	3.60	2.16
010092	6.7	1461±15	1.66	0.00	229	3.61	2.20

is the first time that such low values of crystalline fraction are deduced from spectroscopic ellipsometry measurements.

V. DISCUSSION

Modeling the dielectric function of *a*-Si:H films by BEMA gives an accurate description of the optical properties of the films.[13] However, the effect of hydrogen on the dielectric function is not negligible as shown by the studies of films produced by sputtering in which the hydrogen content can be controlled.[34] On the other hand its effect on the dielectric function has been modeled using the tetrahedron model.[20] In this paper we have used the tetrahedron model combined with the BEMA approximation in order to model the dielectric function of amorphous, polymorphous and protocrystalline silicon. In our application of the tetrahedron model only the $Si–Si_3H$ tetrahedron has been used and the influence of more hydrogenated tetrahedron such as $Si–Si_2H_2$ have been neglected. This approach gives good results only in cases where hydrogen is distributed randomly throughout the silicon network, i.e., when the fraction of $Si–Si_2H_2$ is low and has no influence on the dielectric function [see Fig. 2(a)].

TABLE V. Hydrogen content and void fractions of the films of Table IV obained by ellipsometry, compared to the hydrogen content and film density deduced from ERDA and RBS measurements, respectively.

Total Pressure (Pa)	Deduced %H	Deduced % Cryst.	Deduced %void	ERDA %H	RBS Dens. (g/cm^3)
240	15	0	0	···	···
213	13	0	0.5	15	2.22±0.03
187	14.5	8	1	15	2.21±0.03
93	18	13	3.7	20	2.21±0.03
80	19	15	5.5	20	2.23±0.03
67	25	23	4.5	19	2.24±0.03
53	25	17	4.5	19	2.24±0.03

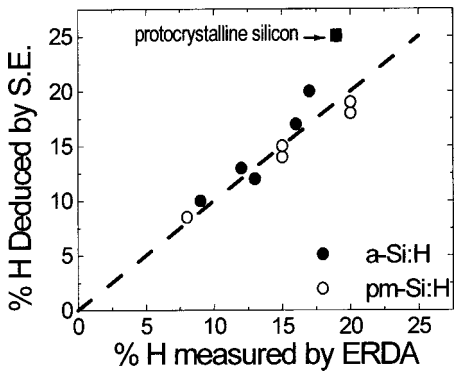

FIG. 10. Correlation between the hydrogen content deduced from the analysis of the spectroscopic ellipsometry data and that obtained by ERDA measurements.

The results on hydrogen content and void fraction presented in Tables III and V show an excellent agreement between the hydrogen content deduced from ellipsometry and that deduced from ERDA measurements except for the films with a crystalline fraction of 17% and 23%, which can be considered as protocrystalline. This is further illustrated in Fig. 10, where we have summarized the results on the hydrogen content for the amorphous and polymorphous films. Indeed, we obtain a linear relation (with a slope of 1) between the hydrogen content deduced from the analysis of the spectroscopic ellipsometry data and the hydrogen content deduced from ERDA measurements. Thus for homogeneous films with hydrogen content up to 20% the tetrahedron model provides a simple way for an accurate estimation of the hydrogen content. As indicated above, there is a deviation from the linear relation for the protocrystalline silicon films as well as for the amorphous silicon sample deposited at 50 °C with a hydrogen content of 18.5% and a void fraction of 11%. This is attributed to hydrogen bonded at the surface of the crystallites or at the surface of voids in the low temperature *a*-Si:H, which is in the form of $Si–Si_2H_2$ and results in a overestimation of the hydrogen content. The excellent agreement obtained for the pm-Si:H films with hydrogen content up to 14.5% supports the hypothesis of an homogeneous structure for this material which has a dense network in spite of its high hydrogen content. This contrasts with our standard *a*-Si:H films (see Table III) as well as with the dependence found for *a*-Si:H films prepared by hot wire CVD.[35] The high density of pm-Si:H films is corroborated by the very low void fraction deduced from spectroscopic ellipsometry.

The obtaining of a dense network with high hydrogen content must be related to the differences in the growth mechanisms between amorphous, polymorphous, and microcrystalline silicon films. Indeed, microcrystalline silicon is an evolving material and the crystallites nucleate in a highly hydrogenated matrix,[36] where hydrogen is concentrated in platelets most likely in the $Si–H_2$ form.[37] On the other side, amorphous and polymorphous silicon grow in a homogeneous way resulting from the incorporation of radicals, clus-

ters and nanocrystals formed in the plasma. Moreover, the dense network of pm-Si:H films results in a slower hydrogen diffusion,[38] required of the growth of the crystallites in the bulk.[39,40] Therefore, the silicon nanocrystals produced in the plasma and incorporated in the amorphous matrix are frozen and the properties of pm-Si:H films are independent of their thickness, in contrast to microcrystalline films for which the crystalline fraction increases with film thickness.

The small size and fraction of the plasma produced silicon crystals makes their detection challenging. Up to now their unambiguous detection could only be done by HRTEM, which requires quite tedious sample preparation and skilled interpretation. For the first time small silicon crystalline fractions ~8% have been detected by SE measurements. The use of the tetrahedron model combined with the BEMA approximation opens the possibility for an easy characterization.

VI. SUMMARY AND CONCLUSIONS

The dielectric functions of amorphous and polymorphous silicon films measured with spectroscopic ellipsometry have been modeled taking into account the effect of hydrogen through the use of the tetrahedron model. The results in terms of hydrogen content and void fraction (density) have been checked against these deduced from ERDA and RBS measurements. Moreover, the introduction of the dielectric function of $Si–Si_3H$ allows a more precise description of the dielectric function of pm-Si:H and thus the detection of crystalline fraction values as low as 8%. The analysis suggests that the structure of pm-Si:H films consists of a dense hydrogen-rich silicon network in which a small fraction of crystallites are embedded. The increase of pressure from 187 to 213 Pa does not result in a significant change in the hydrogen content but results in a decrease of the crystalline fraction from 8% to 0%. The ellipsometry analysis suggests that the high hydrogen content (15%–20%) in pm-Si:H films is randomly distributed throughout the silicon network. As opposed to *a*-Si:H, pm-Si:H films have a high hydrogen content along with a high density, resulting from a different growth mechanism. This is consistent with our previous studies showing that, as opposed to proto and microcrystalline materials, the dielectric function of pm-Si:H films does not change during growth.

As a conclusion, the use of the tetrahedron model combined with BEMA gives a detailed description of amorphous and polymorphous silicon films, confirmed by nuclear measurements. We have shown that this simple approach can be applied to silicon thin films with a wide range of hydrogen content. The unique structure of polymorphous silicon films is characterized by a high density and high hydrogen content, along with the presence of a small crystalline fraction.

ACKNOWLEDGMENTS

This study was partly supported by the European Community under contract *H*-Alpha Solar N.ERK6-CT-1999-00004 and by the Center National de la Recherche Scientifique (CNRS) and the French Agency for Environment and Energy Management (ADEME-Agence de l'Environnement et de la Maîtrise de l'Energie).

*Author to whom correspondence should be addressed. Electronic address: roca@poly.polytechnique.fr

[1] P. Roca i Cabarrocas, S. Hamma, S. N. Sharma, J. Costa, and E. Bertran, J. Non-Cryst. Solids **227–230**, 871 (1998).
[2] P. Roca i Cabarrocas, J. Non-Cryst. Solids **266–269**, 31 (2000).
[3] R. J. Koval, J. M. Pearce, A. S. Ferlauto, R. W. Collins, and C. R. Wronski, IEEE Photovoltaic Specialists Conference, 2000, p. 944.
[4] P. M. Voyles, J. E. Gerbi, M. M. J. Treacy, J. M. Gibson, and J. R. Abelson, Phys. Rev. Lett. **86**, 5514 (2001).
[5] A. Fontcuberta i Morral and P. Roca i Cabarrocas, Thin Solid Films **383**, 161 (2001).
[6] J. Koh, A. S. Ferlauto, P. I. Rovira, C. R. Wronski, and R. W. Collins, Appl. Phys. Lett. **75**, 2286 (1999).
[7] M. Meaudre, R. Meaudre, R. Butté, S. Vignoli, C. Longeaud, J. P. Kleider, and P. Roca i Cabarrocas, J. Appl. Phys. **86**, 946 (1999).
[8] S. Vignoli, R. Butté, R. Meaudre, M. Meaudre, and P. Roca i Cabarrocas, J. Phys.: Condens. Matter **11**, 8749 (1999).
[9] R. Meaudre, R. Butté, S. Vignoli, M. Meaudre, L. Saviot, O. Marty, and P. Roca i Cabarrocas, Eur. Phys. J.: Appl. Phys. **22**, 171 (2003).
[10] A. Fontcuberta i Morral, R. Brenot, E. A. G. Hamers, R. Vanderhaghen, and P. Roca i Cabarrocas, J. Non-Cryst. Solids **266–269**, 48 (2000).
[11] J. P. Kleider, C. Longeaud, M. Gauthier, M. Meaudre, R. Meaudre, R. Butté, S. Vignoli, and P. Roca i Cabarrocas, Appl. Phys. Lett. **75**, 3351 (1999).
[12] O. Saadane, S. Lebib, A. V. Kharchenko, C. Longeaud, and P. Roca i Cabarrocas, J. Appl. Phys. **93**, 9371 (2003).
[13] H. Fujiwara, J. Koh, P. I. Rovira, and R. W. Collins, Phys. Rev. B **61**, 10 832 (2000).
[14] B. Drévillon, Prog. Cryst. Growth Charact. Mater. **27**, 1 (1997).
[15] H. V. Nguyen and R. W. Collins, Phys. Rev. B **47**, 1911 (1993).
[16] P. Roca i Cabarrocas, S. Hamma, S. N. Sharma, J. Costa, and E. Bertran, J. Non-Cryst. Solids **227–230**, 871 (1998).
[17] F. Abèles, *Advanced Optical Techniques*, edited by A. C. S. Van Hell (North-Holland, Amsterdam, 1967).
[18] K. Mui and F. W. Smith, Phys. Rev. B **38**, 10 623 (1988).
[19] D. A. G. Bruggeman, Ann. Phys. (Leipzig) **24**, 636 (1935).
[20] T. Haage, U. I. Schmidt, H. Fath, P. Hess, B. Schröder, and H. Oechsner, J. Appl. Phys. **76**, 4894 (1994).
[21] K. Mui, D. K. Basa, and F. W. Smith, Phys. Rev. B **35**, 8089 (1987).
[22] K. Mui and F. W. Smith, Phys. Rev. B **38**, 10 623 (1988).
[23] N. Layadi, P. Roca i Cabarrocas, B. Drévillon, and I. Solomon, Phys. Rev. B **52**, 5136 (1995).
[24] S. Sriraman, S. Agarwal, E. S. Aydil, and D. Maroudas, Nature (London) **418**, 62 (2002).
[25] B. C. Bagley, D. E. Aspnes, A. C. Adams, and C. J. Mogab, Appl. Phys. Lett. **38**, 56 (1981).
[26] F. Abèles, *Advanced Optical Techniques*, edited by A. C. S. Van Hell (North-Holland, Amsterdam, 1967).
[27] E. D. Palik, *Handbook of Optical Constants of Solids* (Academic, New York, 1991).

[28] D. E. Aspness and J. B. Theeten, J. Electrochem. Soc. **127**, 1359 (1980).
[29] G. E. Jellison Jr. and F. A. Modine, Appl. Phys. Lett. **69**, 371 (1996).
[30] R. J. Severens *et al.*, Mater. Res. Soc. Symp. Proc. **377**, 33 (1995); **420**, 341 (1996).
[31] A. Fontcuberta i Morral, H. Hofmeister, and P. Roca i Cabarrocas, J. Non-Cryst. Solids **299–302**, 284 (2002).
[32] A. Fontcuberta i Morral and P. Roca i Cabarrocas, Thin Solid Films **383**, 161 (2001).
[33] P. Roca i Cabarrocas, A. Fontcuberta i Morral, Sarra Lebib, and Y. Poissant, Pure Appl. Chem. **74**, 359 (2002).
[34] G. F. Feng, M. Katiyar, J. R. Abelson, and N. Maley, Phys. Rev. B **45**, 9103 (1992).
[35] M. Vanecek and A. H. Mahan, J. Non-Cryst. Solids **190**, 163 (1995).
[36] P. Roca i Cabarrocas, Curr. Opin. Solid State Mater. Sci. **6**, 439 (2002).
[37] A. von Keudell and J. R. Abelson, J. Appl. Phys. **84**, 189 (1998).
[38] A. Fontcuberta i Morral and P. Roca i Cabarrocas, J. Non-Cryst. Solids **299–302**, 196 (2002).
[39] C. Godet, N. Layadi, and P. Roca i Cabarrocas, Appl. Phys. Lett. **66**, 3146 (1995).
[40] B. Kalache, A. I. Kosarev, R. Vanderhaghen, and P. Roca i Cabarrocas, J. Appl. Phys. **93**, 1262 (2003).